Available online at www.sciencedirect.com
SCIENCE DIRECT®
International Journal of Heat and Mass Transfer 48 (2005) 331–339
International Journal of HEAT and MASS TRANSFER
www.elsevier.com/locate/ijhmt

Combustion of liquid fuel inside inert porous media: an analytical approach

Tarun K. Kayal, Mithiles Chakravarty *

Chemical Engineering Section, Central Glass & Ceramic Research Institute, Kolkata 700 032, India

Received 22 March 2004; received in revised form 28 July 2004

Abstract

This paper presents a numerical analysis of combustion of liquid fuel droplets suspended in air inside an inert porous media. A one-dimensional heat transfer model has been developed assuming complete vaporization of oil droplets prior to their entry into the flame. The effects of absorption coefficient, emissivity of medium, flame position on radiative energy output efficiency and optimum oil droplet size at the entry, defined as the maximum size for complete vaporization before entering the combustion zone, have been presented. The inert porous medium with low absorption coefficient will produce high downstream radiative output with large oil droplet sizes.

1. Introduction

In the last few decades, porous media burners of gaseous fuel have shown lot of promise over the conventional burners. The premixed gaseous fuel–air mixture is burnt inside the solid porous matrix to release the heat of combustion to heat up the matrix which converts sensible heat of combustion to radiative energy. The radiative energy not only preheats the reactant gas mixture in the upstream section for combustion augmentation but also emits radiation in the downstream end to heat the load. The advantages of porous media burners are high power density, very low emission, very wide power range, combustion stability over wide range of equivalence ratio and high thermal efficiency. These advantages of porous radiative burners have led to their various thermal applications [1,2].

Many combustion models have been developed [3–6] to analyze the combustion characteristics of porous media burner for premixed gaseous fuel–air system. But for combustion of liquid fuel using porous media, only a few experimental and theoretical studies have been reported. Takami et al. [7] studied the combustion behavior of kerosene when the fuel was added drop wise at the top of the porous ceramic plate and ignited at the bottom surface of the plate. Jugjai and Polmart [8] used a set up containing porous ceramic media and packed bed with air mixing chamber in between them. Kerosene was added drop wise to the top of ceramic matrix. Kerosene got vaporized while traveling through porous matrix and met the swirling air in combustion chamber and finally the packed bed was used in the downstream section to convert thermal energy to radiation energy for emission. Temperature profile for both axial and radial position of the set up was measured and analyzed. Fuse et al. [9] used the radiant energy of kerosene flame and

* Corresponding author. Tel.: +91 33 2473 3469; fax: +91 33 2473 0957.
E-mail address: mchakravarty@cgcri.res.in (M. Chakravarty).

0017-9310/$ - see front matter © 2004 Elsevier Ltd. All rights reserved.
doi:10.1016/j.ijheatmasstransfer.2004.08.017

Nomenclature

a	specific area, m^{-1}
A	pre-exponential factor in reaction rate, s^{-1}
Bi	Biot number
c	specific heat of gas at constant pressure, $J kg^{-1} K^{-1}$
c_{pv}	specific heat of oil vapor at constant pressure, $J kg^{-1} K^{-1}$
d	Sauter mean diameter of oil droplet, μm
d^*	optimum Sauter mean diameter of oil droplet, μm
d'	dimensionless diameter of oil droplet, d/d^*
D	diffusion coefficient, $m^2 s^{-1}$
E	activation energy, $J kg mol^{-1}$
E^*	emissivity of solid
E'	downstream radiative efficiency in percent, $q^*(L)/q'$
E''	total radiative efficiency in percent, $[q^*(L) - q^*(0)]/q'$
h	heat transfer coefficient, $W m^{-2} K^{-1}$
i	radiation intensity, $W m^{-2}$
i_b	black body intensity, $W m^{-2}$
k	thermal conductivity, $W m^{-1} K^{-1}$
L	porous layer length, m
L^*	optical thickness, αL
L'	dimensionless preheating temperature zone length, $(x^* - x')/L$
L''	dimensionless effective oil vaporization length, $(x^* - x'')/L$
m	mass of single liquid droplet, kg
M	average molecular weight, $kg mol^{-1}$
M_1, M_2, M_3	dimensionless quantities as in Eq. (17)
n	number density of droplets, m^{-3}
n_f	fuel concentration, $kg mol m^{-3}$
n_{O2}	oxygen concentration, $kg mol m^{-3}$
Nu	Nusselt number
p	pressure, $N m^{-2}$
p_v	partial vapor pressure, $N m^{-2}$
q	radiative heat flux, $W m^{-2}$
q^*	net radiative heat flux, $W m^{-2}$
q'	reaction enthalpy flux, $W m^{-2}$
Q	dimensionless radiative heat flux, $q/(\sigma T_i^4)$
Q^*	dimensionless net radiative heat flux, $q^*/(\sigma T_i^4)$
Q'	dimensionless reaction enthalpy flux, $q'/(\sigma T_i^4)$
R	Universal gas constant, $J kg mol^{-1} K^{-1}$
Re	Reynolds number
s	scattering coefficient, m^{-1}
Sc	Schmidt number
Sh	Sherwood number
T	temperature, K
T_A	autoignition temperature, K
$\bar{T}$	average film temperature, $(T_g + T_l)/2$
T^*	dimensionless gas temperature, $(T_g - T_i)/T_i$
$T^{*\prime}$	dimensionless peak gas temperature, $(T_m - T_i)/T_i$
u	axial velocity, $m s^{-1}$
u_L	laminar burning velocity of stoichiometric oil–air mixture, $m s^{-1}$
V^*	dimensionless burning velocity, u_3/u_L
x	axial coordinate, m
x'	value of x where $T^* = 0.01$
x''	value of x where $p_{vo}/p = 0.01$
x^*	axial coordinate at flame plane, m
X	dimensionless axial coordinate, x/L
X^*	dimensionless axial coordinate at flame plane, x^*/L
y	mass fraction of gaseous product
Y	constant as in Eq. (6)

Greek symbols

α	absorption coefficient, m^{-1}
φ	porosity
ρ	density, $kg m^{-3}$
σ	Stefan–Boltzman constant, $W m^{-2} T^{-4}$
ψ	inertial impaction factor
λ	latent heat of vaporization of oil, $J kg^{-1}$

Superscripts

+	forward direction
−	backward direction

Subscripts

b	boiling point of liquid
e	exit plane
f	flame plane
g	gas
gl	between gas and liquid
gs	between gas and solid
i	inlet
l	liquid
m	maximum
o	droplet surface
s	solid
v	vapor
∞	bulk gas
1, 2, 3, 4	interfacial planes

furnace walls for penetration through porous ceramic plate to vaporize the oil from the oil container for continuous oil vaporization and sustenance of stable combustion. Premixed fuel oil sprayed droplets in air were

used in place of gaseous fuel–air mixture for porous radiant burner using ceramic matrix by several investigators [10,11]. They got stabilized combustion inside the matrix and studied effect of various parameters on the combustion inside the matrix. Martynenko et al. [12] formulated a mathematical model where the oil droplets vaporize inside an inert porous medium with self-sustained combustion of the oil vapor–air mixture. The model considers the behavior of oil droplets which collide and deposit on the porous solid structure and also their effect on heat transfer parameters. Tseng and Howell [13] have conducted both experimental and numerical studies of liquid heptane droplet vaporization and combustion of gaseous mixture inside the inert porous medium made of zirconia. The flashback and blow-off limits of the combustion within the porous structure were determined. It was concluded that smaller droplet size (<25 μm) of heptane could be evaporated in the low temperature region before the flame front.

The present study investigates the thermal behavior of a highly porous ceramic matrix for combustion of premixed sprayed kerosene droplets in air where the liquid droplets are completely vaporized in the low temperature region just before reaching the flame front.

2. Mathematical analysis

2.1. Analytical model

The schematic diagram representing the one-dimensional model under steady state condition is shown in Fig. 1. A mixture of sprayed oil (kerosene) droplets in laminar flow enters an adiabatic duct containing inert porous medium of total length L. The oil–air mixture enters medium ($x = 0$) at temperature T_i. The combustion gas finally leaves the medium through region C at $x = L$ at temperature T_e. The porous medium is divided into three regions A, B and C. The interfacing planes (1, 2, 3 and 4) are perpendicular to x-direction and separating the regions. The radiative heat fluxes in forward and backward directions in the porous medium are q^+ and q^- respectively.

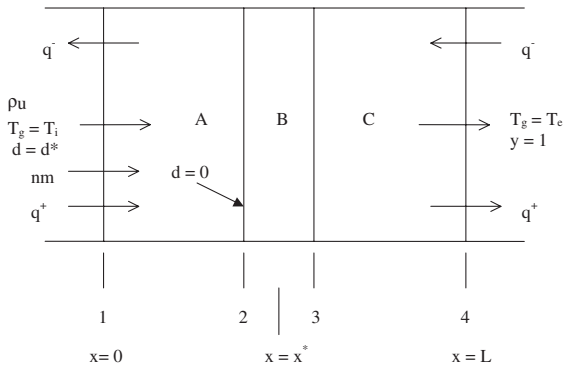

Fig. 1. Schematic diagram of combustion system in a porous medium.

The principal assumptions used in the formulation are as follows:

(a) The working gas is non-radiating.
(b) The structure is having high porosity and the gas flow is laminar so that the pressure drop across the porous medium is negligible.
(c) The porous medium is a homogeneous continuum, the physical properties of which are given by multiplying those of porous material by a factor of $(1 - \varphi)$.
(d) The porous medium is able to emit and absorb radiation in local thermal equilibrium while radiative scattering is ignored.
(e) A one-dimensional radiative propagation occurs in x-direction without any reaction being taken place in regions A and C.
(f) The size of inlet oil droplets (d^*) is optimum such that the vaporization of oil droplets is complete just before entering the combustion region B.
(g) Velocities of air and liquid droplets are same in region A.
(h) No temperature gradient exists inside each droplet.
(i) Physical interaction occurring between porous medium surface and oil droplets suspended in air is negligible.

The assumptions in the region B for the reaction system are:

(j) The porous medium is non-catalytic.
(k) The oil vapor–air mixture enters the region at a temperature $T_g \leqslant T_A$ where T_A is the autoignition temperature of oil vapor–air mixture.
(l) The reaction starts and gets completed in the region at constant temperature $T_g = T_m$.
(m) The medium at interface 2 absorbs radiation as upward radiation flux in region A.
(n) The one-step global irreversible reaction between oil vapor and air is considered.

Some of these assumptions are discussed in details. The assumption (a) is realized as the emissivity of the gas is much less than the porous solid medium. The assumption (b) is justified as the usual matrix structure of radiant burners [6] is in the form of ceramic porous open cellular foams or ceramic fibre structure which has very high porosity in the range of 0.95–0.99. Also low pressure drop across the porous solid is justified due to laminar flow of gas through highly porous solid

medium. The assumption (d) is realized to cover most of the porous medium such as ceramic foam [5] and porous metallic media [3]. The assumption (e) is reasonable due to good thermal insulation outside the duct in presence of negligible radial flow.

The assumptions (f)–(i) need discussions in details. In this study, fine oil droplets ($d < 14\mu$), which are generated usually in air atomizing nozzles [14] in a separate container, enter the porous media so that each droplet gets sufficient time to reach its terminal velocity which is very small in comparison to bulk velocity of air so that the velocity of each droplet is nearly equal to that of air velocity. For such fine droplets, Biot number $[hd/k_l]$ is estimated to be much less than 0.1 so that no temperature gradient can exist within each droplet [15]. For ceramic foam with low pore density (number of pores per inch), the collecting structure [9,16] for aerosol of oil in air is assumed to be cylindrical of average diameter 1.5 mm. Inertial impaction factor (ψ) based on Stokes law for cylindrical target on the flow of aerosol path relevant to the present study has been estimated [17]. The maximum value of $\psi^{1/2}$ is nearly 0.4 which corresponds to inertial impact efficiency of 0.03. With this low collection efficiency of porous structure, the physical interaction of aerosol with porous solid structure is assumed to be insignificant.

The assumptions (k)–(n) are discussed in totality. As the porosity of the solid medium is very high ($\varphi > 0.9$) and the gas mixture flow is laminar, the flow may be assumed to be of plug flow nature. In kerosene–air combustion [18], the one step global reaction rate is given by $k_c = 5 \times 10^{11} \exp[-30{,}000/RT_g][n_f]^{0.25}[n_{O2}]^{1.5}\,\mathrm{gmol\,cm^{-3}\,s^{-1}}$ when n_f and n_{O2} are fuel and oxygen concentration respectively using kerosene ($C_{12}H_{24}$). With peak reaction temperature of this system assumed at 2000 K and 99% completion of reaction under the plug flow condition, the reaction thickness is estimated to be about a fraction of millimeter. This dimension is smaller or nearly equal to the dimension of cavity for highly porous ceramic [5] or metallic structure [4]. With high permeability and porosity of matrix structure, the combustion can be realized as if in open space flow condition in such a small thickness so that the assumption of constant temperature of reaction zone is justified as in assumption (l). The maximum temperature of the gas mixture before it enters the reaction region B is its autoignition temperature, T_A. However the inlet temperature at interface 2 is determined by the absorptivity of the porous medium facing reaction zone temperature, T_m. At steady state, the gas mixture at $T_g \leqslant T_A$ when enters the reaction region instantaneously reaches the reaction temperature T_m because of high reaction enthalpy flux. For methane combustion in porous matrix, the gas entry temperature, T_2 was obtained to be less than T_A [3]. So the assumption (m) is justified as the interface 2 exchanges radiative enthalpy from reaction region B only through emissive/absorptive interaction between reaction temperature T_m and low solid temperature at 2. Other assumptions (j) and (n) are taken for computational simplicity.

2.2. Basic equations

Using above assumptions, the continuity equation for the species, energy equations for both gas, liquid and solid phases are formulated respectively [4,18,19].

In reaction region B,

$$\rho u(\partial y/\partial x) = D\rho(\partial^2 y/\partial x^2) + A\rho(1-y) \times \exp[-E/(RT_m)] \tag{1}$$

where mass production rate of species is in first order Arrhenius form.

In region A

$$\rho uc(\partial T_g/\partial x) = k_g(\partial^2 T_g/\partial x^2) - h_{gl}(n\pi d^2)(T_g - T_l) - h_{gs}a_s(T_g - T_s) \tag{2}$$

$$-n\lambda u_l(\partial m/\partial x) = h_{gl}(n\pi d^2)(T_g - T_l) \tag{3}$$

Equation of state:

$$\rho = pM/(RT_g) \tag{4}$$

In region A, for high rate of vaporization of liquid drops at high gas temperature both mass and heat transfer coefficients are modified incorporating the effect of superheating vapor and bulk flow rate of vapor [18]. The vaporization rate of single liquid drop can be expressed as

$$-u_l(\partial m/\partial x) = \pi \mathrm{d} Dp/(R\bar{T})[\ln\{(p - p_{v\alpha})/(p - p_{vo})\}] \times (2 + 0.6Re^{1/2}Sc^{1/3}) \tag{5}$$

where $\bar{T}$ = mean film temperature of liquid drop = $(T_g + T_l)/2$.

T_l is estimated [18] using following equation

$$T_l = T_g - (\lambda/c_{pv})(e^Y - 1) \tag{6}$$

where $Y = [(c_{pv}Dp)/(R\bar{T}k_g)][Sh/Nu][\ln\{p/(p - p_{vo})\}]$.

In Eqs. (5) and (6), the values of D, k_g, c_{pv} are evaluated at $\bar{T}$ and those of p_{vo} and ρ_l at T_l.

In the present case, $u_l = u$, i.e. $Re_l = 0$ and $Sh = Nu = 2$. Also for high mass ratios of air to fuel, $p_{v\alpha} \approx 0$ and Eq. (5) becomes

$$\partial(d^2)/\partial x = -[(8pD)/(R\bar{T}u\rho_l)][\ln\{p/(p - p_{vo})\}] \tag{7}$$

where $m = \rho_l \pi d^3/6$.

In region C

$$\rho uc(\partial T_g/\partial x) = k_g(\partial^2 T_g/\partial x^2) - h_{gs}a_s(T_g - T_s) \tag{8}$$

In A and C regions, the net radiative heat flux, q^* is related to heat fluxes q^+ and q^- in forward and backward directions as

$$q^* = q^+ - q^- \tag{9}$$

$$\partial q^*/\partial x = k_s(\partial^2 T_s/\partial x^2) + h_{gs}a_s(T_g - T_s) \tag{10}$$

Using two-flux gray radiation approximation [19], the equation of transfer for intensity in each hemisphere is integrated over their respective hemispheres to yield forward and backward intensities i^+ and i^- as

$$\partial i^+/(2\partial x) = -(\alpha + s)i^+ + si^- + \alpha i_b \tag{11}$$

$$-\partial i^-/(2\partial x) = -(\alpha + s)i^- + si^+ + \alpha i_b \tag{12}$$

where i_b is the black body intensity. As each intensity over their respective hemisphere is constant under the two-flux model, Eqs. (11) and (12) are integrated over each hemisphere to yield

$$\partial q^+/(2\partial x) = -(\alpha + s)q^+ + sq^- + \alpha\sigma T_s^4 \tag{13}$$

$$-\partial q^-/(2\partial x) = -(\alpha + s)q^- + sq^+ + \alpha\sigma T_s^4 \tag{14}$$

At the interface 2, the absorptance of solid phase at temperature T_2 for incident black radiation of reaction temperature T_m is equal to the emittance of surface at T_m for electrical non-conductors such as ceramics or metal oxide surfaces in which the monochromatic emittance is independent of temperature [20].

$$\text{At } x = x_2: \quad q^- = E^*\sigma T_m^4 - E^*\sigma T_s^4 \tag{15}$$

Other boundary conditions are

$$\begin{aligned}
&x = 0: \quad T_g = T_i, \quad q^+ = 0, \quad d = d^*\\
&x = x_2 - \Delta x: \quad T_g \leqslant T_A, \quad d = 0\\
&\Delta x \to 0\\
&x = x_2: \quad y = 0, \quad T_g = T_m, \quad d = 0\\
&x = x_3: \quad y = 1, \quad T_g = T_m\\
&x = L: \quad T_g = T_e, \quad q^- = 0
\end{aligned} \tag{16}$$

These equations are transformed into dimensionless form using following dimensionless quantities:

$$\begin{aligned}
&X^* = x^*/L, \quad d' = d/d^*, \quad T^* = (T_g - T_i)/T_i,\\
&M_1 = \rho uc/(\sigma T_i^3) \quad M_2 = k_s/(\sigma T_i^3 L),\\
&M_3 = k_g/(\sigma T_i^3 L), \quad L^* = \alpha L
\end{aligned} \tag{17}$$

The energy balance of the reaction region B is worked out by considering the total reaction heat release rate, sensible enthalpy flux of gas and radiative energy flux at both ends. The overall energy balance is made by equating the total reaction heat release rate to the sum of latent heat absorption loss, sensible enthalpy flux at downstream end, radiation heat losses at upstream and downstream ends. Heat conductive energy fluxes at both ends of porous medium are assumed to be negligible [3].

2.3. Numerical solutions

The governing differential equations with boundary conditions were numerically integrated using collocation method [21]. In this method the differential equations are converted to nonlinear system of equations with assumed polynomial spatial profiles for temperature and heat fluxes. These algebraic equations were solved using computer.

The computation was carried out using kerosene–air system in ceramic porous medium. Taking composition of kerosene as $C_{12}H_{26}$, the properties of $C_{12}H_{26}$ as a function of temperature has been used [18]. The auto-ignition temperature of kerosene, $T_A = 503\,K$ was used. For kerosene–air system, laminar burning velocity, u_L for stoichiometric oil–air mixture at 477 K is taken [22] as $0.40\,ms^{-1}$. The base line data are as follows: $Q' = 1\times10^4$, $T_i = 298\,K$, $f = 1.0$, $L = 0.1\,m$, $\varphi = 0.95$, $c = 1.105\,kJ\,kg^{-1}\,K^{-1}$, $k_g = 0.078\,W\,m^{-1}\,K^{-1}$, $k_s = 0.18\,W\,m^{-1}\,K^{-1}$, $E^* = 0.3$, $h_{gs}a_s = 2\times10^7\,W\,m^{-3}\,K^{-1}$ as estimated [4].

3. Results and discussions

The temperature profiles as a function of X, inside the porous medium, at different optical thicknesses, L^* are shown in Fig. 2, with flame location $X^* = 0.5$. It may be mentioned that L^* ($=\alpha L$) can be changed by varying the absorption coefficient of the porous medium, α while L remains same at 0.1 m. For the same flame location, $X^* = 0.5$, the effects of L^* on the peak temperature, $T^{*\prime}$, burning velocity, V^*, radiative efficiencies, E', E'' and the optimum oil drop diameter, d^* are shown in Fig. 3. The temperatures of gas and solid coincide due to firstly, high value of $h_{gs}a_s$ imposed [4,5] and secondly,

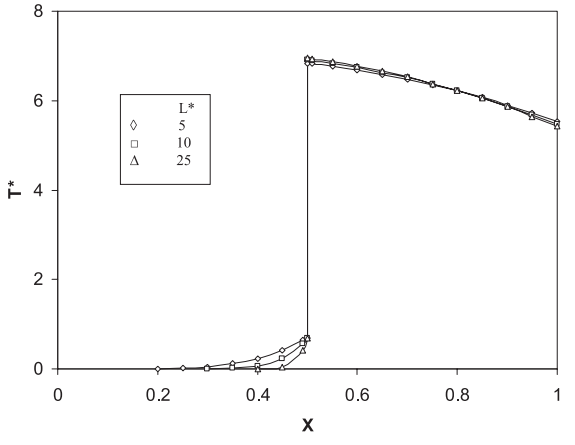

Fig. 2. Gas temperature profiles for several optical thicknesses when $X^* = 0.5$.

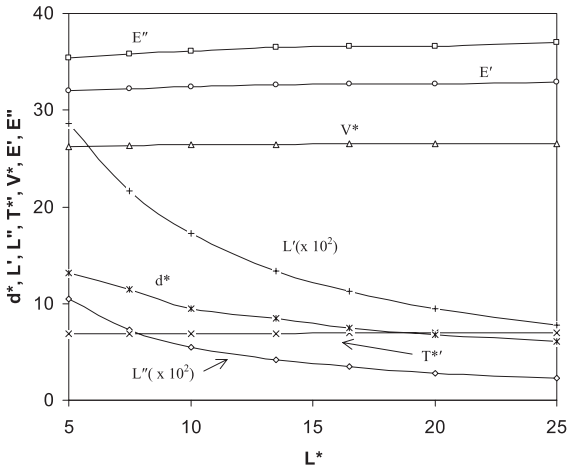

Fig. 3. Radiant output, peak gas temperature, burning velocity, preheating temperature zone length, oil vaporization length and optimum oil droplet diameter for varying optical thicknesses when $X^* = 0.5$.

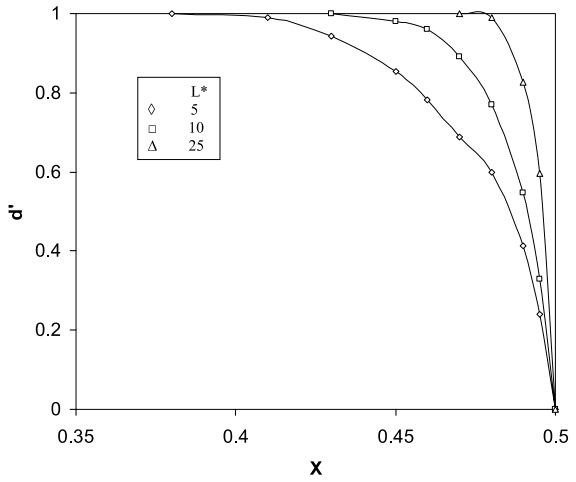

Fig. 4. Oil droplet profiles for different optical thicknesses when $X^* = 0.5$.

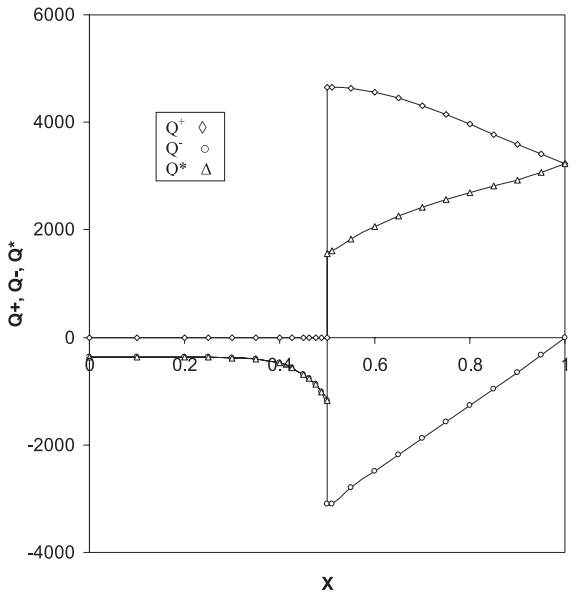

Fig. 5. Profiles in the radiant fluxes in the porous medium for $L^* = 10$, $X^* = 0.5$.

negligible effect of small heat absorbtion rate for vaporization of liquid droplets in comparison to high value of radiative heat flux at any point in the preheating zone. With reaction peak temperature value, $T^{*\prime}$ remaining above 2000 K, the assumption of constant reaction temperature is satisfied. As L^* increases, the increased radiative energy feedback from the post flame region to reaction zone results in increase in V^*. Similar observations have been made earlier [3]. In Fig. 3, variation of L' and L'' with L^* has been shown. Here L', preheating temperature zone length, $(x^* - x')/L$, is defined arbitrarily as the dimensionless distance between $x = x^*$ and $x = x'$ where $T^* = 0.01$ at $x = x'$. It has the physical meaning of T_g just starts increasing above T_i at $x = x'$. L″, effective oil vaporization length, $(x^* - x'')/L$ is similarly defined as the dimensionless distance between $x = x^*$ and $x = x''$ where p_{vo}/p becomes 0.01 at $x = x''$. It means at $x = x''$, the vaporization of oil just starts. For the present system, the value of T_g is nearly equal to 362 K at $x = x''$. With increase in L^*, the preheating temperature zone length, L' and hence the effective oil vaporization length, L'' shorten. So as L^* increases, d^* decreases. With increase in L^*, both downstream and upstream losses start increasing. This indicates that with increase in L^*, the radiative feedback increases from the post flame region towards upstream up to the air entry end. The oil droplet profile as a function of X at $X^* = 0.5$ for different values of L^* are shown in Fig. 4. Sharp changes in d' occur due to sharp change in L' and L'' with increase in L^* as observed in Fig. 3.

The radiative heat fluxes as a function of X in the porous media is presented in Fig. 5 when $X^* = 0.5$. Maximum radiative heat flux exchange occurs at the reaction zone $X^* = 0.5$. This supports the concept of radiative energy feedback in such systems proposed by Weinberg [23]. At the reaction zone, there are sharp changes in forward and backward heat fluxes. At both ends of the porous medium, the net heat fluxes represent heat losses. Similar observations were made by others [3,19].

Fig. 6 shows the effect of position of reaction zone, X^*, on gas temperature distribution. The reaction temperature and the temperature profile do not significantly change in the range of $X^* = 0.2$–0.8 for $L^* = 10$. Variation of $T^{*\prime}$, d^*, V^*, E' and E'' with X^* is shown in

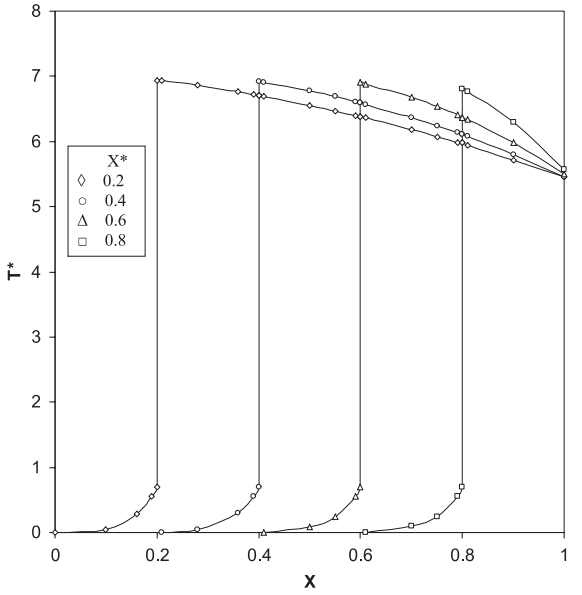

Fig. 6. Gas temperature profiles for several positions of the reaction zone for $L^* = 10$.

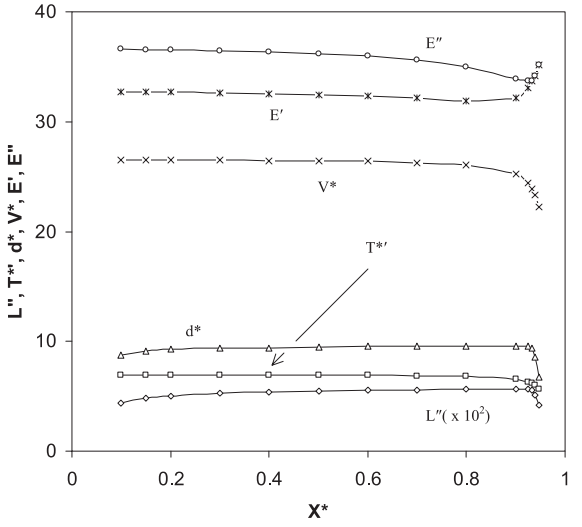

Fig. 7. Radiant output, peak gas temperature, burning velocity, oil vaporization length and optimum oil droplet diameter at several flame locations for $L^* = 10$.

Fig. 7 for $L^* = 10$. In Fig. 8 for various values of L^*, the effect of X^* on d^*, L'' is presented. In Fig. 7 with increase in X^* from 0.1 to 0.925, d^* and the oil vaporization length, L'', increase in a similar fashion. But at $X^* > 0.925$ the sudden decrease in d^* occurs. This is firstly due to decrease in L'' and secondly due to decrease in value of T_2 from T_A. In other words, this is due to shorter vaporization length with lower preheat temperature profile as X^* increases from 0.925 to 0.947. In Fig. 8, variation of d^* with X^* is similar for $L^* = 5$, 10, 25. But as L^* is increased, early change of d^* at $X^* < 0.2$ diminishes as well as highest value of d^*, which occurs at high values of X^*, decreases. In Fig. 7, the shifting of X^* towards the upstream end leads to the increase in upstream radiative end loss whereas the downstream loss is nearly constant for $X^* < 0.9$. With $X^* > 0.925$, the downstream loss starts increasing and upstream loss decreasing sharply and finally becomes zero with $x^* \geqslant 0.93$. In the porous medium, the radiative heat feedback depends on the value of $T^{*\prime}$, V^* and effective upstream optical thickness. This affects $T^{*\prime}$, V^* and the heat losses from both ends.

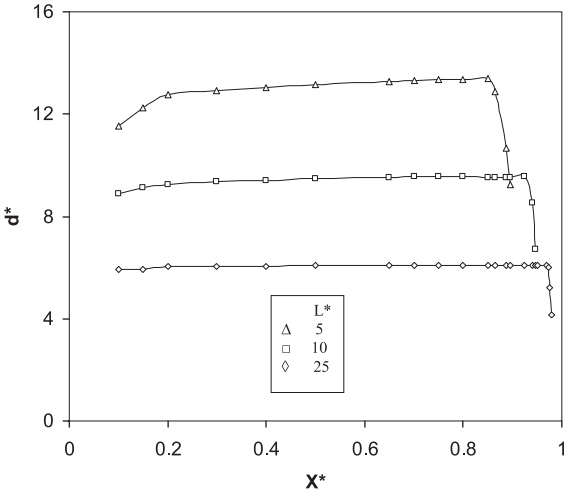

Fig. 8. Effects of position of reaction zone on optimum oil droplet diameter for several optical thicknesses.

The effect of effective emissivity, E^* of the porous medium on its thermal performance is presented in Fig. 9. There is almost no change in $T^{*\prime}$ and V^* with the variation in E^*. d^* remains constant with variation of E^* as the value of T_2 remains at T_A throughout the range of E^*. As E^* increases, the radiative heat losses at the downstream and upstream ends decrease and increase respectively almost in a linear way. This indicates that the emissivity of material of construction of porous medium has a profound effect on thermal performance of system.

Fig. 10 shows the effect of reaction enthalpy flux, Q', on the performance of the system. $T^{*\prime}$ and V^* increase almost proportionately with Q'. The downstream loss, $Q^*(L)$, increases with Q'. E' and E'' decrease sharply with increase in Q'. At low values of Q', the radiative efficiencies are quite high. It shows that at low values of Q', the conversion of sensible heat of gas to radiative heat becomes more efficient whereas at high values of Q', the sensible heat loss in exit gas predominates over the radiative heat feedback. With increase in Q', d^*

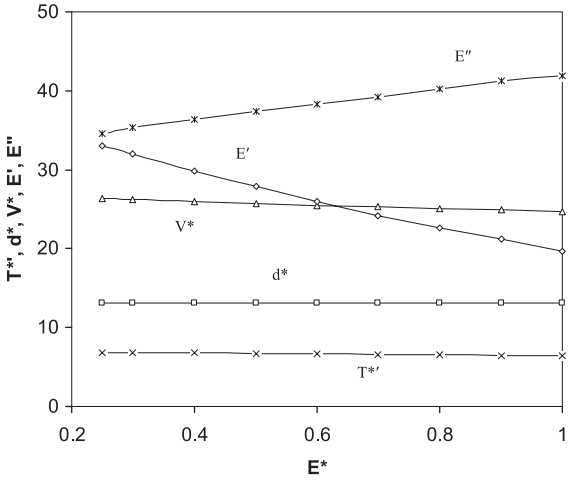

Fig. 9. Effect of emissivity of porous medium on radiative output, peak gas temperature, burning velocity and optimum oil droplet diameter for $L^* = 5$ and $X^* = 0.5$.

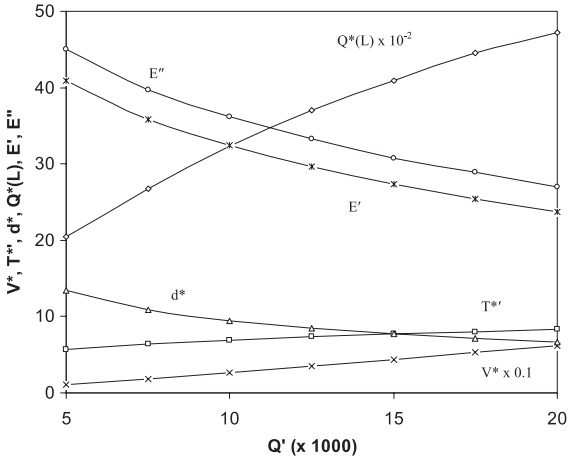

Fig. 10. Effect of reaction enthalpy flux on radiant output, peak gas temperature, burning velocity and optimum oil droplet diameter for $L^* = 10$ and $X^* = 0.5$.

decreases due to the lower preheat temperature profile for high air flow rates.

It can be summarized that the optical thickness, flame position and emissivity play important role in determining the radiative end losses and optimum oil diameter. In an industrial application, the downstream radiative loss is used for thermal applications whereas the upstream radiative loss is undesirable because it is a waste of energy not suitable for safe handling of flammable gases. Also there is limitation in oil spray devices for the generation of fine oil droplets with low power input. The porous system which can handle large inlet droplet size and has high downstream radiative end loss with no upstream loss is desirable. High downstream radiative loss without any upstream loss is obtainable with high values of X^* for combustion process. Large droplet diameter is obtained when the length of preheat temperature zone is large. This is obtained for low values of L^*. So the porous medium with low values of L^* (i.e. low absorption coefficient) with operating flame position more towards downstream end of the porous medium will be the desirable system for combustion of sprayed droplets suspended in air. It may be mentioned that energy consumption for oil breakup to large droplets will be much less in comparison to that required for small droplets.

Acknowledgment

The authors express their sincere gratitude to Dr. H.S. Maiti, Director, CGCRI for his keen interest and encouragement in this work under the Institute project and kind permission to publish this paper.

References

[1] R. Echigo, Effective energy conversion method between gas enthalpy and gas radiation and application to industrial furnaces, in: Proceedings of the Seventh International Heat Transfer Conference, München, 1982, pp. 361–366.
[2] S. Mößbauer, O. Pickenäcker, K. Pickenäcker, D. Trimis, Application of porous burner technology in energy and heat engineering in: Proceedings of the Fifth International Conference on Technologies and Combustion for a Clean Environment (Clean Air V), Lisbon, 1999, pp. 12–15.
[3] Y. Yoshizawa, K. Sasaki, R. Echigo, Analytical study of the structure of radiation controlled flame, Int. J. Heat Mass Transfer 31 (1988) 311–319.
[4] S.B. Sathe, R.E. Peck, T.W. Tong, A numerical analysis of heat transfer and combustion in porous radiant burners, Int. J. Heat Mass Transfer 33 (6) (1990) 1331–1338.
[5] P.F. Hsu, J.R. Howell, R.D. Mathews, A numerical investigation of premixed combustion within porous inert media, Trans. ASME, J. Heat Transfer 115 (1993) 744–750.
[6] D. Trimis, F. Durst, O. Pickenäcker, K. Pickenäcker, Porous medium combustion versus combustion systems with free flame, in: Proceedings of the Second International Symposium on Heat Transfer Enhancement and Energy Conservation, Guangzhou, China, 1997.
[7] H. Takami, T. Suzuki, Y. Itaya, M. Hasatani, Performance of flammability of kerosene and NO_X emission in the porous burner, Fuel 77 (3) (1998) 165–171.
[8] S. Jugjai, N. Polmart, Enhancement of evaporation and combustion of liquid fuels through porous media, Exp. Therm. Fluid Sci. 27 (8) (2003) 901–909.
[9] T. Fuse, Y. Araki, N. Kobayashi, M. Hasatani, Combustion characteristics in oil-vaporizing sustained by radiant heat flux enhanced with higher porous ceramics, Fuel 82 (11) (2003) 1411–1417.

[10] M. Kapalan, M.J. Hall, The combustion of liquid fuels within a porous media radiant burner, Exp. Therm. Fluid Sci. 11 (1) (1995) 13–20.
[11] F. Durst, M. Keppler, M. Weclas, Air-assisted nozzle applied to very compact, ultra-low emission porous medium oil-burner, in: Proceedings of the Third Workshop (Spray 97), Lampoldshausen, 1997.
[12] V.V. Martynenko, R. Echigo, H. Yoshida, Mathematical model of self-sustaining combustion in inert porous medium with phase change under complex heat transfer, Int. J. Heat Mass Transfer 41 (1) (1998) 117–126.
[13] C.-J. Tseng, J.R. Howell, Combustion of liquid fuels in porous radiant burner, Combust. Sci. Technol. 112 (1996) 141–161.
[14] A.J. Teller, Liquid–gas systems, in: R.H. Perry, C.H. Chilton, S.D. Kirkpatrick (Eds.), Chemical Engineer' Handbook, fourth ed., McGraw-Hill, New York, 1963, pp. 18–68.
[15] P.J. Schneider, Conduction, in: W.M. Rohsenow, J.P. Hartnett (Eds.), Handbook of Heat Transfer, McGraw-Hill, New York, 1973, pp. 3–37.
[16] P.F. Hsu, W.D. Evans, J.R. Howell, Experimental and numerical study of premixed combustion within non-homogeneous porous ceramics, Combust. Sci. Technol. 90 (1993) 149–172.
[17] W. Strauss, Industrial Gas Cleaning, Pergamon Press, London, 1966, p. 219.
[18] G.L. Borman, K.W. Ragland, Combust. Eng., McGraw-Hill, New York, 1998, pp. 323, 374, 570.
[19] S.W. Baek, The premixed flame in a radiatively active porous medium, Combust. Sci. Technol. 64 (1989) 277–287.
[20] E.R.G. Eckert, R.M. Drake Jr., Analysis of Heat and Mass Transfer, McGraw-Hill, New York, 1972, p. 612.
[21] P. Razelos, Methods of obtaining approximate solutions, in: W.M. Rohsenow, J.P. Hartnett (Eds.), Handbook of Heat Transfer, McGraw-Hill, New York, 1973, pp. 4–72.
[22] M.W. Thring, The Science of Flames and Furnaces, Chapman and Hall, London, 1962, p. 226.
[23] F.J. Weinberg, Combustion temperatures: the future, Nature 233 (5317) (1971) 239–241.